ACS Sustainable Chemistry & Engineering

pubs.acs.org/journal/ascecg

Research Article

Anomalous Facile Carbamate Formation at High Stripping Temperatures from Carbon Dioxide Reaction with 2-Amino-2-methyl-1-propanol in Aqueous Solution

Bohak Yoon and Gyeong S. Hwang*

Cite This: *ACS Sustainable Chem. Eng.* 2020, 8, 18671−18677

Read Online

ACCESS | Metrics & More | Article Recommendations | Supporting Information

ABSTRACT: Based on first-principles simulations, we present that carbamate formation can be kinetically more favorable than bicarbonate formation at high stripping temperatures (>400 K) from the reaction between CO_2 and 2-amino-2-methyl-1-propanol (AMP) in aqueous solution, while the latter tends to be predominant during CO_2 capture at low absorber temperatures (<330 K). This finding offers explanation for the intriguing observation of oxazolidinone formation as the major product of AMP degradation, which is known to occur via carbamate, as also seen from thermal degradation of aqueous monoethanolamine (MEA) in CO_2 capture processes. From *ab initio* molecular dynamics simulations coupled with metadynamics sampling, the free-energy barrier for carbamate formation is predicted to substantially decrease from 11.7 to 5.5 kcal/mol with increasing temperature from 313 to 413 K in 25 wt % AMP solution whereas that for bicarbonate formation increases from 9.6 to 12.4 kcal/mol. Likewise, the predicted free-energy barrier for carbamate formation in aqueous MEA also decreases with temperature but is significantly less compared to the AMP case. Further analysis demonstrates that the increase of temperature results in enhancing the disruption of the hydrogen bond network around the basic nitrogen atom of AMP (or MEA), allowing more facile CO_2 access to form carbamate. Our work provides new insight on the strong temperature dependence of the CO_2 capture mechanism and kinetics in aqueous solutions of amines, arising from changes in the hydrogen bond structure and dynamics around amines.

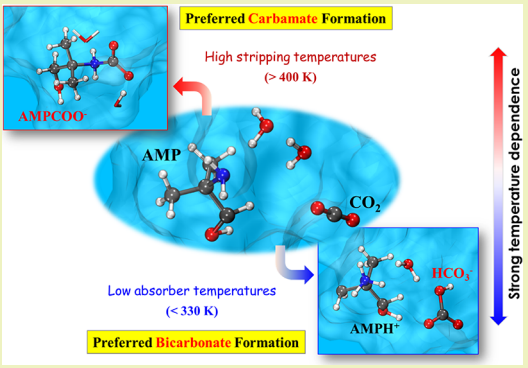

KEYWORDS: *2-amino-2-methyl-1-propanol, CO_2 capture mechanism, hydrogen bond dynamics, ab initio molecular dynamics, metadynamics*

INTRODUCTION

Chemical absorption using aqueous amine solutions is currently the most widely used method for carbon dioxide (CO_2) capture from post-combustion flue gases of coal-fired power plants.[1,2] While monoethanolamine (MEA), a simple and cheap primary amine, is considered as the benchmark solvent, 2-amino-2-methyl-1-propanol (AMP), a sterically hindered primary amine, has been proposed as a commercially attractive alternative because of its high CO_2 loading capacity and relatively fast absorption rate, in addition to low degradation and corrosion rates.[3−5]

From previous experiments, it is now well known that bicarbonate is the predominant product of CO_2 capture by aqueous AMP under absorber conditions.[3,6] In addition, recent first-principles studies have revealed that bicarbonate formation via amine-catalyzed hydrolysis can be kinetically more favorable than carbamate formation at relatively low absorber temperatures (<330 K).[7] The strong hydrogen bonding interaction between nitrogen of AMP and an adjacent water molecule tends to suppress the direct reaction of CO_2 with AMP leading to carbamate formation while facilitating the bicarbonate reaction route.[8,9] According to recent experimental studies,[10,11] AMP may undergo thermal degradation at high stripping temperatures while its main degradation product is found to be 4,4-dimethyl-1,3-oxazolidin-2-one (DMOZD). To explain the DMOZD formation, it has been suggested that AMP could form carbamate ($AMPCOO^-$) by reacting with CO_2,[12] similar to the case of MEA. The mechanism for oxazolidinone production via $MEACOO^-$ has been well illustrated by recent first-principles studies, which is also consistent with experimental observations.[13,14] This raises an intriguing question regarding the relative favorability of carbamate formation over bicarbonate formation in aqueous

Received: September 29, 2020
Revised: November 19, 2020
Published: December 9, 2020

AMP, especially the possible effect of temperature and its origin.

In this study, we examine whether the mechanism and kinetics of CO_2 capture by aqueous amines are strongly affected by temperature. Using *ab initio* molecular dynamics (AIMD) simulations coupled with metadynamics sampling, we first determine the temperature dependence of free-energy barriers for both carbamate and bicarbonate formation reactions in aqueous AMP. For comparison, the change in barrier height with temperature for carbamate formation in aqueous MEA is also estimated. We also analyze the structure and dynamics of hydrogen bonds between amines and surrounding water molecules at varying temperatures and evaluate their impact on the accessibility of CO_2 to a reactive nitrogen site leading to carbamate formation. The systematic investigation provides insight into the temperature effect and its origin on the reaction of CO_2 in aqueous amine solutions.

COMPUTATIONAL METHODS

Density functional theory (DFT)-based *ab initio* molecular dynamics (AIMD) simulations under the Born−Oppenheimer approximation were performed using the Vienna *Ab initio* Simulation Package (VASP)[15] and the CP2K program package.[16] The generalized gradient approximation (GGA) functionals of Perdew, Berke, and Ernzerhof (PBE)[17] and revised PBE (revPBE)[18] were used in AIMD simulations with VASP and CP2K, respectively. The projector-augmented wave (PAW) method[19] was used to treat core and valence electrons in VASP calculations. Norm-conserving Goedecker−Teter−Hutter (GTH) pseudopotentials[20] were employed to describe the interactions between ionic cores and valence electrons in CP2K simulations. A hybrid Gaussian and plane waves (GPW) scheme[21] was implemented in the QUICKSTEP module[22] of CP2K in which atom-centered Gaussian-type orbitals were used to describe the wave functions and an auxiliary plane wave basis set for expansion of the electron density. We employed a triple-ζ Gaussian basis set with two sets of polarization functions (TZV2P) in CP2K and a plane wave kinetic energy cutoff (E_{cut}) of 400 Ry (400 eV) in CP2K (VASP). The Brillouin zone was sampled using only the gamma point, given the lack of structural symmetry in aqueous solutions studied. The choices of E_{cut} and *k*-point sampling were carefully checked to ensure convergence of the calculations (see Figure S1 and Table S1 in the Supporting Information). The long-range van der Waals interaction was included via the semi-empirical corrections by Grimme D3 (DFT-D3),[23] which is known to minimize the excess ordering of the liquid structure and significantly improve the liquid state of water.[24] To integrate the equations of motion, a time step of 0.5 *FS* was used. In NVT simulations, the temperature was controlled by a velocity rescaling thermostat with a temperature coupling time constant of 300 *FS*.[25] All hydrogen atoms were replaced by deuterium in CP2K simulations. Each system was equilibrated for 5 ps before the production run. A well-tempered algorithm[26] was employed in metadynamics simulations,[27] as implemented in PLUMED[28] with CP2K. Gaussian hills with an initial hill height of 1.13 kcal/mol and a width of 0.04 Å were deposited at a rate of 10^{-4} FS^{-1} with the height decay set by ΔT = 3500 K. More details on the computational methodologies including convergence of the metadynamics simulations and confirmation of associated transition states of a free-energy landscape can be found in the Supporting Information (Figures S2 and S3).

RESULTS AND DISCUSSION

Temperature Dependence of Free-Energy Barriers. We first assessed free-energy surfaces for the formation of bicarbonate through amine-catalyzed hydration of CO_2, i.e., AMP + H_2O + CO_2 → $AMPH^+$ + HCO_3^-, at both absorber and stripper temperatures (∼40 and ∼140 °C) using well-tempered metadynamics-biased AIMD. In prior, various test runs were carefully analyzed to obtain optimal bias parameters of the metadynamics method, such as the hill height, width, and frequency of the deposited Gaussian potential. H_2O (30), AMP (2), and CO_2 (1) molecules were placed in a cubic box of side 10.57 Å with periodic boundary conditions, corresponding to 25 wt % AMP solution with 0.5 CO_2 loading with a density of 1.04 g/cm^3 (close to an experimental value[29]). Here, the free-energy surface was computed, considering (i) the protonation/deprotonation of the $-NH_2$ group in AMP and (ii) the formation/dissociation of the C−O bond between OH^- and CO_2. Two independent collective variables (CVs) used are (i) the bond−distance-dependent coordination number of a proton bound to the base N atom in AMP (CN_{N-H}), mimicking protonation of AMP (AMP + H_2O → $AMPH^+$ + OH^-), and (ii) the coordination number that mimics the C−O bond formation (CN_{C-O}), leading to bicarbonate formation (CO_2 + OH^- ↔ HCO_3^-). For the *CN* computations, the N−H and C−O bond distances are set at 1.1 and 1.5 Å, respectively, beyond which the bonds are assumed to break. CN_{N-H} and CN_{C-O} have a value close to unity in the protonation of the $-NH_2$ group and the formation of bicarbonate, respectively, while they are zero in the initial state. The *CN*-based CVs may provide a better description of bond formation/dissociation compared to those based on the relative distances between the atoms involved in the reaction.[30] A more detailed information regarding the choice of CVs can be found in the Supporting Information.

Figure 1 shows the free-energy surface (ΔA) as a function of CN_{N-H} and CN_{C-O}, together with snapshots of the initial, transition, and final states. At the initial state (*IS*), both CN_{N-H} and CN_{C-O} are zero, indicating that AMP and CO_2 are fully separated with no significant interaction. CN_{N-H} increases substantially to 0.5, while CN_{C-O} changes only by 0.1 at the transition state (*TS*), implying that the amine-catalyzed reaction is initiated primarily by proton abstraction from H_2O by AMP. Both CN_{N-H} and CN_{C-O} are 1 at the final state (*FS*), indicating that the AMP + H_2O + CO_2 → $AMPH^+$ + HCO_3^- reaction is completed. According to the computed free-energy surface in Figure 1, the reaction barrier for the bicarbonate formation is estimated to be 9.6 kcal/mol at 313 K, which is slightly higher than 8.1 kcal/mol from previous metadynamics simulations[9] with different CVs, and increases

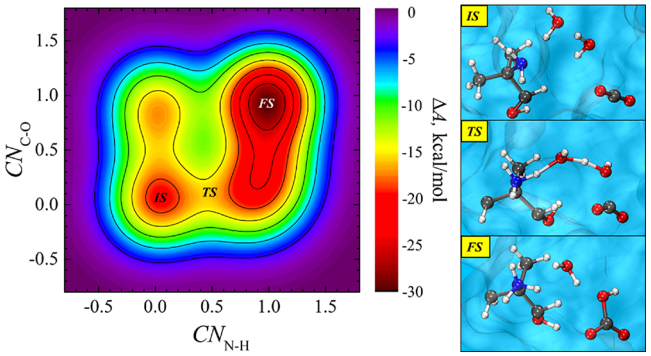

Figure 1. Free-energy surface (ΔA in kcal/mol) for bicarbonate formation via amine-catalyzed hydrolysis, i.e., AMP + CO_2 → $AMPH^+$ + HCO_3^-, predicted by metadynamics simulations at 313 K. Shown at the right are the structures of the initial (*IS*), transition (*TS*), and final (*FS*) states in which the blue, red, gray, and white balls represent N, O, C, and H atoms, respectively.

https://dx.doi.org/10.1021/acssuschemeng.0c07203
ACS Sustainable Chem. Eng. 2020, 8, 18671−18677

to 12.4 kcal/mol at 413 K. The increased free-energy barrier, albeit not substantially, suggests that the AMP-catalyzed bicarbonate formation could be kinetically hindered, to a certain extent, with increasing the solution temperature.

We then also evaluated the temperature dependence of the free-energy profile for a competing reaction leading to carbamate formation. Here, the direct reaction of CO_2 with AMP forming a zwitterionic intermediate, i.e., AMP + CO_2 → $AMP^+CO_2^-$, is only considered using the distance between N of AMP and C of CO_2 (d_{C-N}) as a CV. The free-energy barrier for the carbamate formation is primarily determined by the zwitterion formation since the successive deprotonation reaction may occur with no sizable barrier. Hence, the single CV, d_{C-N}, should be suitable and sufficient to describe the free-energy variation along the corresponding reaction coordinate.

As shown in Figure 2, a relatively large d_{C-N} of 2.7 Å at the *IS* allows separation of CO_2 and AMP with no intermolecular

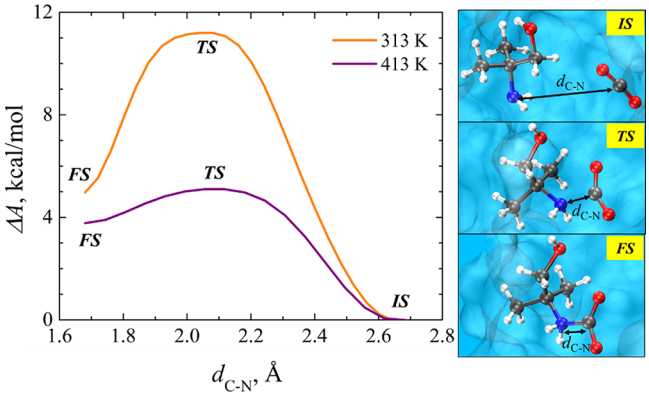

Figure 2. Predicted free-energy profiles (ΔA) for the reaction of CO_2 with AMP to form carbamate by metadynamics simulations at 313 and 413 K, as indicated. Shown at the right are the structures of the initial (*IS*), transition (*TS*), and final (*FS*) states in which the blue, red, gray, and white balls represent N, O, C, and H atoms, respectively.

bonding interaction between the lone pair on N (in AMP) and electrophilic C atom (in CO_2). As d_{C-N} decreases, the C−O bonds of CO_2 are elongated while the CO_2 structure becomes substantially bent due to the electron transfer from the N lone pair of AMP to CO_2.[31] d_{C-N} is 2.1 Å at the *TS* and further decreases to 1.7 Å at the *FS*. From the short-lived zwitterion at the *FS*, a proton tends to be released almost instantaneously to form carbamate. At 313 K, a predicted free-energy barrier of 11.7 kcal/mol is higher than 9.6 kcal/mol for bicarbonate formation. However, interestingly, the carbamate formation barrier drops significantly to 5.5 kcal/mol while the bicarbonate formation barrier increases to 12.4 kcal/mol as the solution temperature is increased to 413 K. The results clearly demonstrate that carbamate formation can be kinetically more favorable than bicarbonate formation at high stripping temperatures (~413 K). For comparison, we also calculated the free-energy barriers for carbamate formation in aqueous MEA using metadynamics simulations with the same procedure as the AMP case; the resulting barriers are 7.9 and 6.8 kcal/mol at 313 and 413 K, respectively (see Figure S5).

We further performed AIMD simulations to verify the temperature dependence of the major kinetic pathway for CO_2 capture in aqueous AMP. In each simulation, 25 H_2O, 1 AMP, and 1 CO_2 molecules were placed in a cubic box of side 10.12 Å with periodic boundary conditions. During about a 40 ps simulation, we only observed a carbamate formation at 413 K via the direct reaction between AMP and CO_2, as illustrated in Figure 3. The electrophilic C of CO_2 is attacked by the lone

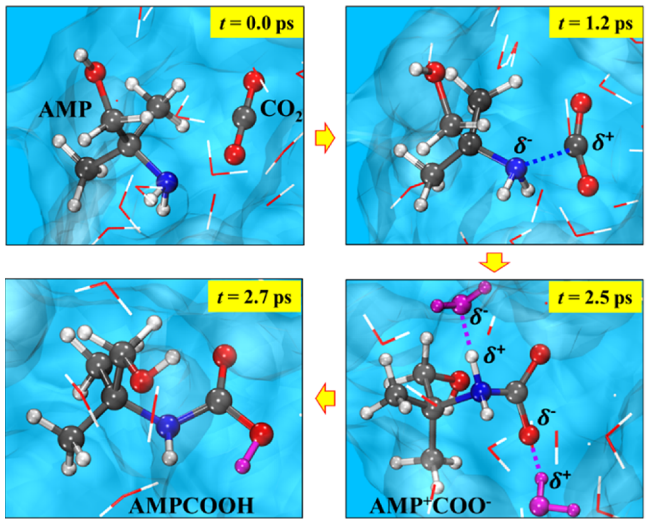

Figure 3. AIMD snapshots representing the reaction between AMP and CO_2, leading to carbamic acid formation at 413 K. The blue, red, gray, and white balls represent N, O, C, and H atoms, respectively. H_2O molecules directly involved in the associated proton transfer are shown in purple.

pair of N in AMP [(a) → (b)] followed by short-lived zwitterionic intermediate formation [(b) → (c)] and subsequent deprotonation [(c) → (d)]; here, the proton released from the zwitterion is abstracted by the carbamate group to form carbamic acid, but the protonation of free AMP, if it is available, is thermodynamically more favorable, i.e., 2 AMP + CO_2 → $AMPCOO^-$ + $AMPH^+$.[7] At 313 K, as illustrated in Figure S6, one H_2O molecule remains bound to N of AMP for 11 ps, hindering CO_2 accessibility, which has also been well demonstrated in previous studies.[7−9] Due to the limited simulation time, bicarbonate formation was not observed from six independent runs at both 313 and 413 K. Nonetheless, our simulation is sufficient to prove relative ease of carbamate formation at 413 K, which appears to be closely related to the dynamics of H_2O molecules surrounding the $-NH_2$ group. In the following section, we examine how temperature affects the dynamics of the interaction between the $-NH_2$ group of AMP and surrounding H_2O molecules, with a comparison to the MEA case.

Hydrogen Bond Structure and Dynamics. Previous studies[13,32] demonstrate that, compared to the MEA case, the N atom of AMP forms a stronger hydrogen bond (HB) with an adjacent H_2O molecule. The relatively strongly bound H_2O is thought to be mainly responsible for the suppression of carbamate formation by hindering the accessibility of CO_2 to the N site while facilitating bicarbonate formation via base-catalyzed hydration of CO_2.[7−9] Hence, we first evaluated the disruption of the HB between N in amine and H in neighboring H_2O by calculating a continuous HB autocorrelation function, $S(t)$, which describes the probability that the hydrogen-bonded N···H pair remains bonded at all times up to time t. The average HB lifetime, τ_S, is obtained by integrating $S(t)$. A more detailed description of the calculations can be found in the Supporting Information.

https://dx.doi.org/10.1021/acssuschemeng.0c07203
ACS Sustainable Chem. Eng. 2020, 8, 18671−18677

As summarized in Figure 4, a predicted τ_S of 14.5 ps in the AMP solution is about twice longer than 6.9 ps, as predicted in

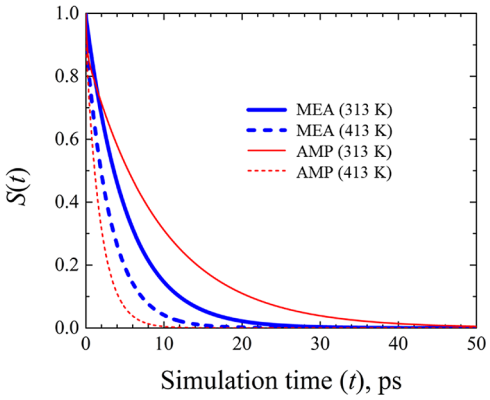

Figure 4. Continuous hydrogen bond autocorrelation functions for a H_2O molecule bonded to the N atom of AMP (thin red lines) or MEA (thick blue lines) at 313 and 413 K, from AIMD simulations. Here, 34 H_2O, 2 AMP (or MEA), and 1 CO_2 molecules were placed in a cubic simulation box of side 11.40 Å with periodic boundary conditions.

the MEA solution at 313 K, consistent with previous studies.[7,32] However, the increase of solution temperature to 413 K results in a significant reduction of τ_S yielding 3.3 ps in the AMP case, which is even smaller than 5.1 ps in the MEA case. The reduced τ_S may adversely affect the proton abstraction from an adjacent H_2O molecule, which could explain the increase in the predicted barrier for bicarbonate formation from 9.6 to 12.4 kcal/mol with increasing temperature from 313 to 413 K (see Figure 1). Moreover, the N site of AMP could become more available for the direct reaction with CO_2 to form carbamate. In addition, the HB network around $-NH_2$ of AMP is predicted to be more disrupted at 413 K, even when compared to the MEA case (*vide infra*). As a result, CO_2 accessibility for binding to the N site of AMP would be less hindered, allowing for facile carbamate formation as well as demonstrated by the significant decrease of the corresponding free-energy barrier (see Figure 2).

We further analyzed the dynamics of H_2O molecules surrounding MEA and AMP through computation of changes in the diffusivity and dipole moment with varying temperatures. Table 1 summarizes calculated diffusion coefficients

Table 1. Predicted Water Diffusion Coefficients ($\times 10^{-5}$ cm^2/s) by AIMD Simulations[a]

system	T = 313 K	T = 413 K
2 AMP, 1 CO_2, 34 H_2O	1.7	3.8
2 MEA, 1 CO_2, 34 H_2O	2.0	3.2
pure H_2O	2.1 (2.4*)	3.1

[a]The asterisk (*) indicates the experimental value from ref 32.

(D_{H2O}) and average dipole moments for H_2O in aqueous MEA and AMP solutions at 313 and 413 K; the calculated values of D_{H2O} and the dipole moment for pure water are also included for comparison. Here, D_{H2O} is estimated from a mean squared displacement (MSD) using the Einstein relation $D_{H2O} = \langle MSD \rangle / 6t$ [$= \langle | R_i(t) - R_i(0)|^2 \rangle / 6t$], where $R_i(t)$ denotes the position of atom i at time t, and the angle bracket indicates an ensemble average. For each system, $\langle MSD \rangle$ was determined from an AIMD production run of 25 ps after a 5 ps equilibration run; the plots of MSD versus t are presented in Figure S7 (Supporting Information). At 313 K, D_{H2O} tends to decrease from 2.1×10^{-5} cm^2/s in pure water to 2.0×10^{-5} and 1.7×10^{-5} cm^2/s in the MEA and AMP solutions, respectively. On the other hand, H_2O is predicted to become more mobile in the AMP solution ($D_{H2O} = 3.8 \times 10^{-5}$ cm^2/s) at 413 K, as compared to the cases of the MEA solution ($D_{H2O} = 3.2 \times 10^{-5}$ cm^2/s) and pure water ($D_{H2O} = 3.1 \times 10^{-5}$ cm^2/s).

It is well known that molecular solutes exert a strong effect on the structure and dynamics of water surrounding them through perturbation of H-bonding networks. At low temperatures, the H-bond disruption may cause an enhancement of local structural ordering and a decrease in mobility. In particular, the H_2O molecules surrounding $-NH_2$ of AMP are confined to a certain degree by the hydrophobic methyl groups, leading to the formation of strong H-bonds between the $-NH_2$ group and neighboring H_2O molecules; the resulting mobility restriction can be well demonstrated by the enhanced structural rigidity. Therefore, as presented in Table 1, the decrease of D_{H2O} in the AMP solution at 313 K, as compared to pure water, tends to be more substantial than that in the MEA solution. As the solution temperature increases, the enhanced perturbation of H-bonding networks may contribute to an increase in D_{H2O}. The temperature dependence of structural disruption is well expected to become stronger in the presence of molecular solutes; this can explain the greater increase of D_{H2O} with temperature in the MEA and AMP solutions, as compared to the case of pure water. Our results also imply that the extent of H-bond disruption would be greater in the AMP solution due mainly to the hydrophobic methyl groups, yielding higher D_{H2O}, as compared to the MEA and pure water cases.

To better understand the effects of the solvent and temperature on the H-bond structure and dynamics, we calculated the dipole moment of H_2O molecules in pure water and aqueous solutions of MEA and AMP at two different temperatures (313 and 413 K) using the maximally localized Wannier function (MLWF) method.[33] The centers of MLWFs can be treated as quasiparticles, and the molecular dipole moment can be computed in a classical way by integrating the positions and electrical charges of the nuclei and MLWF centers of H_2O.[34] Here, MLWF centers were evaluated at every fifth AIMD step (2.5 *FS*). The description of the calculations are explained in more detail in the Supporting Information.

The dipole moment of a H_2O molecule arises from the electronegativity difference between O and H and is enhanced by forming H-bonds. The enhancement of the dipole moment depends on the local H-bond structure. At room temperature, the average dipole moment of H_2O molecules in pure water is calculated to be 2.94 Debye (D), which is close to an experimental value of 2.91 D[35] and in good agreement with previous theoretical studies.[36−39] Figure 5 shows dipole moment distributions of water in the MEA and AMP solutions, giving average values of 2.81/2.87 and 2.66/2.55 D in the former/latter case at 313 and 413 K, respectively. For both AMP and MEA solutions, the dipole moment decreases as compared to pure water and further decreases with increasing temperature. The dipole moment decrease is apparently due to the reduction of the H-bond strength arising from H-bond disruption. At 313 K, a slightly higher dipole moment of 2.87

https://dx.doi.org/10.1021/acssuschemeng.0c07203
ACS Sustainable Chem. Eng. 2020, 8, 18671−18677

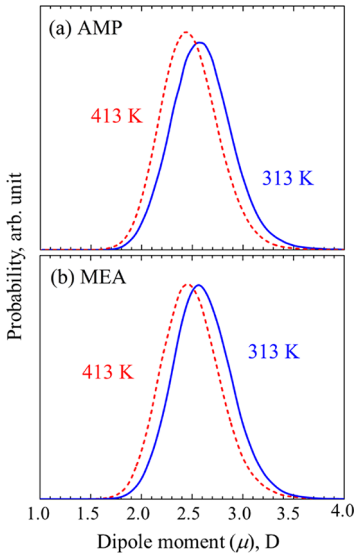

Figure 5. Dipole moment distributions of water in (a) AMP solution and (b) MEA solution at 313 (solid blue) and 413 K (dashed red), from AIMD simulations with the same conditions, as employed in Figure 4.

D in the AMP solution, relative to 2.81 D in the MEA solution, indicates that H_2O molecules are more strongly H-bonded and thus less mobile. On the other hand, the relatively smaller dipole moment at 413 K implies that the H-bonds are more disrupted in the AMP solution than in the MEA solution, consistent with the analysis of H_2O diffusion.

Temperature Effect on CO_2 Accessibility. To evaluate the temperature effect on CO_2 accessibility, we computed the radial distribution function between N in AMP or MEA and C of CO_2, which is given by $g(r) = \langle n(r, r + dr)/4\pi r^2 \rho dr \rangle$, where $n(r, r + dr)$ is the number of C in a spherical shell of radius r with a thickness dr from the reference N, or vice versa, and ρ is the bulk number density. The $g(r)$ for each case was obtained from an average of five independent systems with different initial configurations. As shown in Figure 6, the lower tail of $g(r)$ is substantially shifted to the right as MEA is replaced with AMP at 313 K, indicating that the CO_2 access to the N site is significantly inhibited in the AMP solution, as discussed earlier. With increasing temperature to 413 K, however, the $g(r)$ tail is considerably shifted down and the first peak intensity becomes much greater in the AMP case, implying that CO_2 more easily

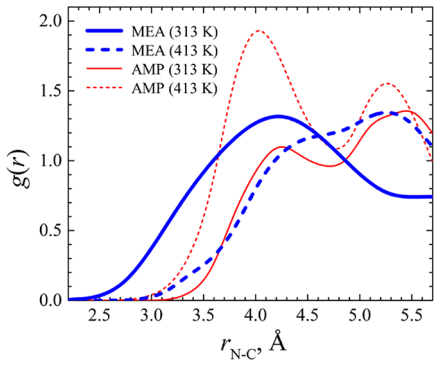

Figure 6. Radial distribution functions between N in AMP (or MEA) and C of CO_2 at two different temperatures as specified, from AIMD simulations with the same conditions, as employed in Figure 4.

approaches and favorably exists around the N site; the opposite trend is predicted for the MEA case. This analysis demonstrates that the increase of temperature may allow facile CO_2 access to form carbamate, which is primarily responsible for the strong temperature dependence of the free-energy barrier for carbamate formation in aqueous AMP, as presented in Figure 2. Our results highlight that carbamate formation can be kinetically more favorable than bicarbonate formation at high stripping temperatures, while the latter tends to be predominant in relatively low absorber temperatures.

CONCLUSIONS

We examined the temperature dependence of the preferred reaction mechanism and kinetics for CO_2 capture in aqueous AMP. The free-energy barriers for two competing reactions leading to bicarbonate or carbamate formation were predicted at high stripping and low absorber temperatures using AIMD metadynamics simulations. To better understand the strong temperature effect, we also analyzed the dynamics of local hydrogen-bonding structures around each amine at varying temperatures and its impact on CO_2 accessibility to the amine's N atom. Our important findings are summarized as follows:

- The free-energy barrier for carbamate formation is predicted to considerably decrease from 11.7 to 5.5 kcal/mol with increasing temperature from 313 to 413 K in 25 wt % AMP solution at 0.5 CO_2 loading. On the other hand, the corresponding barrier height for bicarbonate formation tends to increase from 9.6 to 12.4 kcal/mol. In comparison, the predicted free-energy barriers for carbamate formation in aqueous MEA are 7.9 and 6.8 kcal/mol at 313 and 413 K, respectively, under similar simulation conditions. The results clearly demonstrate that carbamate formation becomes easier with temperature, but the opposite trend is true for bicarbonate formation. As a consequence, carbamate formation can become kinetically more favorable than bicarbonate formation at high stripping temperatures, from the reaction of CO_2 with AMP in aqueous solution.
- The lifetime of the hydrogen bond between N in AMP and H in neighboring H_2O was evaluated and found to be substantially reduced with temperature. At 313 K, the predicted average value (τ_S) is 14.5 ps in the AMP solution considered, which is about twice larger than 6.9 ps in the corresponding MEA solution. However, the increase of temperature to 413 K results in a significant reduction of τ_S yielding 3.3 ps in the AMP case, which is even smaller than 5.1 ps in the MEA case. The reduced τ_S may adversely affect bicarbonate formation via the base-catalyzed hydration of CO_2, explaining the barrier increase with temperature in aqueous AMP.
- Our further analysis based on H_2O diffusivity and dipole moment clarifies stronger disruption of the hydrogen bond networks around AMP compared to MEA at 413 K, attributed primarily to the hydrophobic methyl groups. As a result, the N atom of AMP becomes more accessible to CO_2 for carbamate formation, responsible for the significant reduction in the corresponding barrier height.

Our work highlights that CO_2 reaction dynamics in aqueous solutions of amines can be strongly affected by the temperature-dependent hydrogen bond structure and dynamics

https://dx.doi.org/10.1021/acssuschemeng.0c07203
ACS Sustainable Chem. Eng. 2020, 8, 18671−18677

around amines. The enhanced understanding may provide more complete explanations for experimental observations and also valuable hints on how to optimize existing solvents and design more cost-efficient ones.

■ ASSOCIATED CONTENT

Supporting Information

The Supporting Information is available free of charge at https://pubs.acs.org/doi/10.1021/acssuschemeng.0c07203.

Further computational details and supplementary calculations supporting the findings of this work; detailed descriptions of quantum mechanical calculations, metadynamics simulations, and hydrogen bond correlation function and dipole moment calculations; and predicted free-energy profiles for carbamate formation in aqueous MEA and mean squared displacements of H_2O in aqueous AMP and MEA at 313 and 413 K (PDF)

■ AUTHOR INFORMATION

Corresponding Author

Gyeong S. Hwang − *McKetta Department of Chemical Engineering, University of Texas at Austin, Austin, Texas 78712, United States;* orcid.org/0000-0002-5538-9426; Phone: 1-512-471-4847; Email: gshwang@che.utexas.edu; Fax: 1-512-471-7060

Author

Bohak Yoon − *McKetta Department of Chemical Engineering, University of Texas at Austin, Austin, Texas 78712, United States*

Complete contact information is available at: https://pubs.acs.org/10.1021/acssuschemeng.0c07203

Notes

The authors declare no competing financial interest.

■ ACKNOWLEDGMENTS

This work was supported by the Korea CCS R&D Center (KCRC) grant (no. 2017M1A8A1072016) funded by the Korea government (Ministry of Science, ICT and Future Planning) and the R.A. Welch Foundation (no. F-1535). We would like to thank the Texas Advanced Computing Center for use of the Stampede supercomputing system (OCI-1134872).

■ REFERENCES

(1) Rochelle, G. T. Amine Scrubbing for CO_2 Capture. *Science* **2009**, *325*, 1652−1654.

(2) Mondal, M. K.; Balsora, H. K.; Varshney, P. Progress and Trends in CO_2 Capture/Separation Technologies: A Review. *Energy* **2012**, *46*, 431−441.

(3) Sartori, G.; Savage, D. W. Sterically Hindered Amines for Carbon dioxide Removal from Gases. *Ind. Eng. Chem. Fundam.* **1983**, *22*, 239−249.

(4) Chakraborty, A. K.; Astarita, G.; Bischoff, K. B. CO_2 Absorption in Aqueous Solutions of Hindered Amines. *Chem. Eng. Sci.* **1986**, *41*, 997−1003.

(5) Lepaumier, H.; Picq, D.; Carrette, P.-L. New Amines for CO_2 Capture. I. Mechanisms of Amine Degradation in the Presence of CO_2. *Ind. Eng. Chem. Res.* **2009**, *48*, 9061−9067.

(6) Alper, E. Reaction Mechanism and Kinetics of Aqueous Solutions of 2-Amino-2-Methyl-1-Propanol and Carbon Dioxide. *Ind. Eng. Chem. Res.* **1990**, *29*, 1725−1728.

(7) Stowe, H. M.; Vilčiauskas, L.; Paek, E.; Hwang, G. S. On the Origin of Preferred Bicarbonate Production from Carbon Dioxide (CO_2) Capture in Aqueous 2-Amino-2-Methyl-1-Propanol (AMP). *Phys. Chem. Chem. Phys.* **2015**, *17*, 29184−29192.

(8) Stowe, H. M.; Hwang, G. S. Molecular Insights into the Enhanced Rate of CO_2 Absorption to Produce Bicarbonate in Aqueous 2-Amino-2-Methyl-1-Propanol. *Phys. Chem. Chem. Phys.* **2017**, *19*, 32116−32124.

(9) Stowe, H. M.; Hwang, G. S. Fundamental Understanding of CO_2 Capture and Regeneration in Aqueous Amines from First-Principles Studies: Recent Progress and Remaining Challenges. *Ind. Eng. Chem. Res.* **2017**, *56*, 6887−6899.

(10) Matin, N. S.; Thompson, J.; Onneweer, F. M.; Liu, K. Thermal Degradation Rate of 2-Amino-2-Methyl-1-Propanol to Cyclic 4,4-Dimethyl-1,3-Oxazolidin-2-One: Experiments and Kinetics Modeling. *Ind. Eng. Chem. Res.* **2016**, *55*, 9586−9593.

(11) Matin, N. S.; Thompson, J.; Onneweer, F. M.; Liu, K. Thermal Degradation Rate of 2-Amino-2-Methyl-1-Propanol to Cyclic 4,4-Dimethyl-1,3-Oxazolidin-2-One; Mechanistic Aspects and Kinetics Investigation. *Ind. Eng. Chem. Res.* **2017**, *56*, 9437−9445.

(12) Barzagli, F.; Mani, F.; Peruzzini, M. Efficient CO_2 Absorption and Low Temperature Desorption with Non-Aqueous Solvents Based on 2-Amino-2-Methyl-1-Propanol (AMP). *Int. J. Greenhouse Gas Control* **2013**, *16*, 217−223.

(13) Yoon, B.; Stowe, H. M.; Hwang, G. S. Molecular Mechanisms for Thermal Degradation of CO_2-Loaded Aqueous Monoethanolamine Solution: A First-Principles Study. *Phys. Chem. Chem. Phys.* **2019**, *21*, 22132−22139.

(14) Rochelle, G. T. Thermal Degradation of Amines for CO_2 Capture. *Curr. Opin. Chem. Eng.* **2012**, *1*, 183−190.

(15) Kresse, G.; Furthmüller, J. Efficient Iterative Schemes for Ab Initio Total-Energy Calculations Using a Plane-Wave Basis Set. *Phys. Rev. B* **1996**, *54*, 11169−11186.

(16) Hutter, J.; Iannuzzi, M.; Schiffmann, F.; Vandevondele, J. CP2K: Atomistic Simulations of Condensed Matter Systems. *WIREs Comput. Mol. Sci.* **2014**, *4*, 15−25.

(17) Perdew, J. P.; Burke, K.; Ernzerhof, M. Generalized Gradient Approximation Made Simple. *Phys. Rev. Lett.* **1996**, *77*, 3865−3868.

(18) Zhang, Y.; Yang, W. Comment on "Generalized Gradient Approximation Made Simple". *Phys. Rev. Lett.* **1998**, *80*, 890.

(19) Kresse, G.; Joubert, D. From Ultrasoft Pseudopotentials to the Projector Augmented-Wave Method. *Phys. Rev. B* **1999**, *59*, 1758−1775.

(20) Goedecker, S.; Teter, M.; Hutter, J. Separable Dual-Space Gaussian Pseudopotentials. *Phys. Rev. B* **1996**, *54*, 1703−1710.

(21) Lippert, G.; Hutter, J.; Parrinello, M. A Hybrid Gaussian and Plane Wave Density Functional Scheme. *Mol. Phys.* **1997**, *92*, 477−488.

(22) Vandevondele, J.; Krack, M.; Mohamed, F.; Parrinello, M.; Chassaing, T.; Hutter, J. Quickstep: Fast and Accurate Density Functional Calculations Using a Mixed Gaussian and Plane Waves Approach. *Comput. Phys. Commun.* **2005**, *167*, 103−128.

(23) Goerigk, L.; Grimme, S. A Thorough Benchmark of Density Functional Methods for General Main Group Thermochemistry, Kinetics, and Noncovalent Interactions. *Phys. Chem. Chem. Phys.* **2011**, *13*, 6670−6688.

(24) Gillan, M. J.; Alfè, D.; Michaelides, A. Perspective: How Good Is DFT for Water? *J. Chem. Phys.* **2016**, *144*, 130901.

(25) Bussi, G.; Donadio, D.; Parrinello, M. Canonical Sampling through Velocity Rescaling. *J. Chem. Phys.* **2007**, *126*, No. 014101.

(26) Barducci, A.; Bussi, G.; Parrinello, M. Well-Tempered Metadynamics: A Smoothly Converging and Tunable Free-Energy Method. *Phys. Rev. Lett.* **2008**, *100*, No. 020603.

(27) Laio, A.; Parrinello, M. Escaping Free-Energy Minima. *Proc. Natl. Acad. Sci. U. S. A.* **2002**, *99*, 12562−12566.

(28) Bonomi, M.; Branduardi, D.; Bussi, G.; Camilloni, C.; Provasi, D.; Raiteri, P.; Donadio, D.; Marinelli, F.; Pietrucci, F.; Broglia, R. A.; et al. PLUMED: A Portable Plugin for Free-Energy Calculations with Molecular Dynamics. *Comput. Phys. Commun.* **2009**, *180*, 1961−1972.

(29) Sherman, B. J.; Rochelle, G. T. Thermodynamic and Mass-Transfer Modeling of Carbon Dioxide Absorption into Aqueous 2-Amino-2-Methyl-1-Propanol. *Ind. Eng. Chem. Res.* **2017**, *56*, 319−330.
(30) Galib, M.; Hanna, G. Mechanistic Insights into the Dissociation and Decomposition of Carbonic Acid in Water via the Hydroxide Route: An Ab Initio Metadynamics Study. *J. Phys. Chem. B* **2011**, *115*, 15024−15035.
(31) Stirling, A. HCO_3^- Formation from CO_2 at High pH: Ab Initio Molecular Dynamics Study. *J. Phys. Chem. B* **2011**, *115*, 14683−14687.
(32) Yoon, B.; Hwang, G. S. On the Mechanism of Predominant Urea Formation from Thermal Degradation of CO_2-Loaded Aqueous Ethylenediamine. *Phys. Chem. Chem. Phys.* **2020**, *22*, 17336−17343.
(33) O'Regan, D. D.; Payne, M. C.; Mostofi, A. A. Generalized Wannier Functions: A Comparison of Molecular Electric Dipole Polarizabilities. *Phys. Rev. B* **2012**, *85*, 193101.
(34) Silvestrelli, P. L.; Parrinello, M. Structural, Electronic, and Bonding Properties of Liquid Water from First Principles. *J. Chem. Phys.* **1999**, *111*, 3572−3580.
(35) Badyal, Y. S.; Saboungi, M.-L.; Price, D. L.; Shastri, S. D.; Haeffner, D. R.; Soper, A. K. Electron Distribution in Water. *J. Chem. Phys.* **2000**, *112*, 9206−9208.
(36) Bankura, A.; Karmakar, A.; Carnevale, V.; Chandra, A.; Klein, M. L. Structure, Dynamics, and Spectral Diffusion of Water from First-Principles Molecular Dynamics. *J. Phys. Chem. C* **2014**, *118*, 29401−29411.
(37) Pestana, L. R.; Marsalek, O.; Markland, T. E.; Head-Gordon, T. The Quest for Accurate Liquid Water Properties from First Principles. *J. Phys. Chem. Lett.* **2018**, *9*, 5009−5016.
(38) Schwegler, E.; Grossman, J. C.; Gygi, F.; Galli, G. Towards an Assessment of the Accuracy of Density Functional Theory for First Principles Simulations of Water. II. *J. Chem. Phys.* **2004**, *121*, 5400−5409.
(39) Allesch, M.; Schwegler, E.; Gygi, F.; Galli, G. A First Principles Simulation of Rigid Water. *J. Chem. Phys.* **2004**, *120*, 5192−5198.

https://dx.doi.org/10.1021/acssuschemeng.0c07203
ACS Sustainable Chem. Eng. 2020, 8, 18671−18677